

# A likelihood-based reconstruction algorithm for top-quark pairs and the KL Fitter framework

Johannes Erdmann<sup>a,b</sup>, Stefan Guindon<sup>a,c</sup>, Kevin Kröniger<sup>a</sup>, Boris Lemmer<sup>a</sup>, Olaf Nackenhorst<sup>a</sup>, Arnulf Quadt<sup>a</sup>, Philipp Stolte<sup>a</sup>

<sup>a</sup>*II. Physikalisches Institut, Georg-August-Universität, Göttingen, Germany*

<sup>b</sup>*Now at: Department of Physics, Yale University, New Haven, CT, United States of America*

<sup>c</sup>*Now at: Department of Physics, SUNY Albany, Albany, NY, United States of America*

---

## Abstract

A likelihood-based reconstruction algorithm for arbitrary event topologies is introduced and, as an example, applied to the single-lepton decay mode of top-quark pair production. The algorithm comes with several options which further improve its performance, in particular the reconstruction efficiency, i.e., the fraction of events for which the observed jets and leptons can be correctly associated with the final-state particles of the corresponding event topology. The performance is compared to that of well-established reconstruction algorithms using a common framework for kinematic fitting. This framework has a modular structure which describes the physics processes and detector models independently. The implemented algorithms are generic and can easily be ported from one experiment to another.

*Keywords:*

kinematic fit, top-quark physics, top-quark reconstruction

---

## 1. Introduction

Top quarks are produced abundantly at the LHC. Their production mechanisms as well as their properties are the focus of intensive studies, exploiting the excellent performance of the ATLAS and CMS detectors.

Due to the short lifetime of top quarks, their properties can only be studied indirectly based on their decay products and their corresponding signatures in the detector, i.e. jets, charged leptons and missing transverse

momentum. The full reconstruction of the top-quark four-momenta is necessary for a number of precision measurements, for example measurements of the top-quark mass [1, 2] and of differential distributions [3, 4]. It can also be beneficial for searches for rare processes involving top quarks, for example  $t\bar{t}H$ -production. However, jets cannot be associated uniquely to the partons of the hard-scattering process and hence reconstruction algorithms are used to find the best corresponding match between them. Inefficiencies in these reconstruction algorithms result in *combinatorial background* which may decrease the precision of a measurement.

The aim of this publication is to introduce a likelihood-based method for kinematic fitting and to compare its performance to that of alternative reconstruction algorithms. Reconstruction efficiencies and properties of the reconstructed objects are studied based on a sample of simulated top-quark pairs produced at a proton-proton collider at a center-of-mass energy of  $\sqrt{s} = 7\text{ TeV}$  and decaying to a final state containing exactly one electron. Muons are not considered for reasons of simplicity. The detector response is simulated by smearing the particle energies with assumed resolution functions. All reconstruction algorithms are implemented in a common framework for kinematic fitting, the *Kinematic Likelihood Fitter (KLFitter)*.

Section 2 describes the event signature of the studied process and introduces three reconstruction algorithms. The KLFitter framework is briefly described in Section 3. The Monte Carlo sample used in this study and the detector modeling applied are presented in Section 4, followed by the event selection in Section 5. The performances of the different reconstruction algorithms are compared in Section 6. The last section concludes the paper and gives an outlook on the performance of kinematic fitting of top-quark pairs produced at a center-of-mass energy of  $\sqrt{s} = 14\text{ TeV}$ .

## 2. Event signatures and reconstruction algorithms

Top quarks decay to a  $W$  boson and a bottom quark in nearly 100% of all cases. Consequently, the final state of a top-quark pair is characterized by the decay products of the two  $W$  bosons. If one of the  $W$  bosons decays into a charged lepton and a neutrino while the other one decays into a pair of quarks, the decay mode is referred to as the *single-lepton decay mode*. The fraction of top-quark pairs decaying either in the single-electron or single-muon decay mode is about 30%. The corresponding event signature is defined by exactly one electron or muon, four jets out of which two con-

tain a  $B$  hadron, and a large amount of missing transverse momentum due to the undetected neutrino. Figure 1 shows an example of a leading-order Feynman diagram of top-quark pair production and the subsequent decay in the single-lepton decay mode.

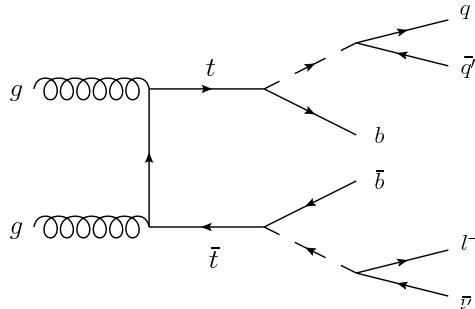


Figure 1: Example of a leading-order Feynman diagram of top-quark pair production and the subsequent decay in the single-lepton decay mode [5].

In the following, we will only refer to quarks in the context of the hard-scattering process, or on the *parton level*. These quarks will hadronize and build showers of stable particles, which we will refer to as the *particle jets* or the *particle level*. It is naively expected that the four quarks on the parton level will result in four particle-level jets. However, additional radiation and jet merging can lead to more or less jets, respectively. Detector effects can further reduce the number of jets observable in a detector, or on the *reconstruction level*. In hadron colliders, additional interactions (pile-up) can increase the number of reconstructed jets. The aim of the reconstruction algorithms is to find the correct association between the reconstructed jets and the particle-level jets.

In the current example, only four jets are used for the reconstruction of the top-quark pair. Other jets, e.g., from initial- and final-state radiation, are ignored (see Section 5 for further details of the event selection). This results in  $4! = 24$  possible ways to associate a reconstructed jet with a particle-level jet, referred to as *permutations* in the following. None of the three algorithms described in this paper is sensitive to a commutation of the two jets from the hadronically decaying  $W$  boson, so the number of distinguishable permutations reduces to 12.

The likelihood-based reconstruction method is described in the following

as well as the two commonly used algorithms, the  $p_T^{\max}$ -method [6, 7] and the  $\chi^2$ -method [8]. While the former algorithm was used to estimate the sensitivity of several ATLAS measurements, variants of the latter are currently in use at Tevatron and LHC experiments. All three algorithms are based on a simplified leading-order picture of the physics processes in which no distinction is made between the particle-level jets and the parton-level quarks. In addition, the  $\chi^2$ - and likelihood methods include terms which describe the mapping between particle-level and reconstructed jets, i.e. taking into account detector resolution effects. Details on the detector model are given in Section 4.

### 2.1. The $p_T^{\max}$ -method

For a given set of three (out of the four) jets, the transverse momentum of the three-jet system is calculated. The set with the largest transverse momentum,  $p_T^{\max}$ , is associated with the decay products of the hadronically decaying top quark while the remaining jet is identified with the  $b$ -jet from the leptonically decaying top quark.

### 2.2. The $\chi^2$ -method

A  $\chi^2$  variable<sup>1</sup> is minimized for each permutation of jets, defined as

$$\begin{aligned}
\chi^2 &= 8 \cdot \ln 2 \cdot \frac{(m_{q_1 q_2 q_3} - m_{\text{top}})^2}{\Gamma_{\text{top}}^2} + 8 \cdot \ln 2 \cdot \frac{(m_{q_1 q_2} - m_W)^2}{\Gamma_W^2} \\
&+ 8 \cdot \ln 2 \cdot \frac{(m_{q_4 \ell \nu} - m_{\text{top}})^2}{\Gamma_{\text{top}}^2} + 8 \cdot \ln 2 \cdot \frac{(m_{\ell \nu} - m_W)^2}{\Gamma_W^2} \\
&- 2 \cdot \sum_{i=1}^4 \ln W_{\text{jet}}(E_{\text{jet},i}^{\text{meas}} | E_{\text{jet},i}) - 2 \cdot \ln W_{\ell}(E_{\ell}^{\text{meas}} | E_{\ell}) \\
&- 2 \cdot \ln W_{\text{miss}}(E_x^{\text{miss}} | p_x^{\nu}) - 2 \cdot \ln W_{\text{miss}}(E_y^{\text{miss}} | p_y^{\nu}), \tag{1}
\end{aligned}$$

and the permutation with the smallest  $\chi^2$  is chosen as an estimate of the correct association of the jets to the final-state particles. The free parameters of the  $\chi^2$  are the mass of the top quark,  $m_{\text{top}}$ , the particle-jet energies,

---

<sup>1</sup>Several definitions for such a  $\chi^2$  variable can be found in the literature, some of which are solved iteratively using Lagrangian multipliers [9]. The version chosen in this paper is closely related to the likelihood defined in Section 2.3.

$E_{\text{jet},i}$  ( $i = 1, \dots, 4$ ), and the energy of the charged lepton,  $E_\ell$ . The first (second) two terms in the first (second) row represent the Gaussian constraints on the hadronic (leptonic) decay branch of the event, where  $m_W = 80.4$  GeV is the mass of the  $W$  boson, and  $\Gamma_{\text{top}} = 1.5$  GeV and  $\Gamma_W = 2.1$  GeV are the decay widths of the top quark and the  $W$  boson, respectively.<sup>2</sup> The expressions  $m_{q_1q_2q_3}$ ,  $m_{q_1q_2}$ ,  $m_{q_4\ell\nu}$  and  $m_{\ell\nu}$  are invariant masses calculated from the reconstructed particles' four-momenta. The last terms in the  $\chi^2$  constrain the particle energies based on the measured energies,  $E_{\text{jet},i}^{\text{meas}}$  ( $i = 1, \dots, 4$ ) and  $E_\ell^{\text{meas}}$ . These terms are referred to as *transfer functions* which in this case are assumed to have a Gaussian shape (see Section 4 for a detailed discussion). Additionally,  $W_{\text{miss}}(E_{x/y}^{\text{miss}}|p_{x/y}^\nu)$  is the transfer function for the  $x$ - and  $y$ -components of the missing transverse momentum,  $E_T^{\text{miss}}$ , and the components of the neutrino momentum. The angles of the particle jets and the charged lepton are assumed to be measured with negligible uncertainty.

Two different options of the  $\chi^2$ -method concerning the treatment of the components of the neutrino momentum are tested. For the first option,  $p_x^\nu$  and  $p_y^\nu$  are determined from the transverse momentum balance of all considered particles in a leading-order approach, thus constraining the transverse momentum of the top-quark pair to zero. The  $z$ -direction of the neutrino momentum,  $p_z^\nu$ , is calculated using a constraint on the  $W$ -boson mass, i.e., solving the equation

$$m_W^2 = (p_\nu + p_\ell)^2 \quad (2)$$

for  $p_z^\nu$ . Here,  $p_\nu$  and  $p_\ell$  are the four-momenta of the neutrino and the charged lepton, respectively. In case two solutions exist, the one with the smaller  $\chi^2$  is chosen. If no solution exists, the longitudinal momentum is set to 0 GeV.

The second option treats the momentum components of the neutrino as additional free parameters. The free transverse momentum components  $p_x^\nu$  and  $p_y^\nu$  allow the  $p_T$  of the top-quark pair to float during the fit.

### 2.3. The likelihood-based method

A likelihood,

$$L = B(m_{q_1q_2q_3}|m_{\text{top}}, \Gamma_{\text{top}}) \cdot \exp\left(-4 \cdot \ln 2 \cdot \frac{(m_{q_1q_2} - m_W)^2}{\Gamma_W^2}\right)$$

---

<sup>2</sup>The prefactors of the first four terms are due to the conversion of the full width at half maximum into standard deviations:  $\Gamma = 2\sqrt{2 \ln 2} \cdot \sigma$ .

$$\begin{aligned}
& \times B(m_{q_4\ell\nu}|m_{\text{top}}, \Gamma_{\text{top}}) \cdot B(m_{\ell\nu}|m_W, \Gamma_W) \\
& \times \prod_{i=1}^4 W_{\text{jet}}(E_{\text{jet},i}^{\text{meas}}|E_{\text{jet},i}) \cdot W_{\ell}(E_{\ell}^{\text{meas}}|E_{\ell}) \\
& \times W_{\text{miss}}(E_x^{\text{miss}}|p_x^{\nu}) \cdot W_{\text{miss}}(E_y^{\text{miss}}|p_y^{\nu}), \tag{3}
\end{aligned}$$

is maximized for each permutation. The functions  $B$  represent Breit-Wigner functions. The free parameters are the same as for the  $\chi^2$ -method plus the three momentum components of the neutrino, corresponding to the second minimization option of the  $\chi^2$ -method. The transfer functions are not constrained to have a Gaussian shape, see Section 4 for their parameterization.

In a naive leading-order picture, all jets are associated with partons. The pole masses of the top quark and the  $W$  boson should then be described by Breit-Wigner functions. On the stable-particle level, this association between jets and partons is not directly possible due to parton showering and hadronization. For the studies presented here, we use an approximation for which we replace the Breit-Wigner term of the hadronically decaying  $W$  boson by a Gaussian term as used for the  $\chi^2$ -method in order to constrain  $m_{q_1q_2}$  to the mass of the  $W$  boson. This approximation is justified by the finite energy resolution of the jets, resulting in a variation of the jet energies over a broad range of values. As a consequence, a Breit-Wigner function with its distinct tails would accept large fluctuations of the reconstructed hadronic  $W$ -boson mass based on these jet energies. Thus, a stronger constraint, as, e.g., provided by a Gaussian term, is chosen. Besides, this procedure leads to the best reconstruction efficiencies found empirically: a fit using the likelihood-based method with only Breit-Wigner function or with only Gaussian terms leads to smaller reconstruction efficiencies than the chosen combination of Breit-Wigner and Gaussian terms. Thus other options are not taken into account for the detailed studies presented in Section 6.1.

Several extensions to the likelihood defined in Equation (3) are available in the current implementation of this method. These are not used in the direct comparison of the three reconstruction methods, but the gain in performance is evaluated separately, see Section 6. The extensions are:

*b-tagging.* In most cases,  $b$ -tagged jets – jets which are identified to stem from a  $b$  quark – do not originate from the light quarks of the hadronically decaying  $W$  boson. Permutations which include such an association are vetoed. When considering exactly four jets in the fit, the number of possible permutations

reduces to six (two) for events with one (two)  $b$ -tags. Events with more than two  $b$ -tagged jets are rejected in the current example because they are not in agreement with the leading-order interpretation of the event topology.

*Fixed top-quark mass parameter.* The mass of the top quark is fixed to the value used in the generation of the Monte Carlo sample.

*Angular information.* The decay of the top quark is described by the  $(V - A)$ -structure of the electroweak interaction predicting the angular distribution of the charged lepton. The angle  $\theta^*$  is defined as the angle between the charged lepton and the reverse momentum direction of the top quark, both in the rest frame of the  $W$  boson. The angular distribution is multiplied by the likelihood,

$$\begin{aligned} \frac{1}{\Gamma_W} \frac{d\Gamma_W}{d\cos(\theta^*)} &= 0.687 \cdot \frac{3}{4} (1 - \cos^2(\theta^*)) + 0.311 \cdot \frac{3}{8} (1 - \cos(\theta^*))^2 \\ &+ 0.002 \cdot \frac{3}{8} (1 + \cos^2(\theta^*)) . \end{aligned} \quad (4)$$

The numerical coefficients used for the longitudinal, left-handed and right-handed  $W$  boson are those given in Ref. [10]. A corresponding (and symmetrized) term for the hadronically decaying  $W$  boson is also added.

### 3. The KLFFitter framework

All three reconstruction methods are implemented in the KLFFitter framework, a C++ program for kinematic fitting based on the Bayesian Analysis Toolkit (*BAT*) [11]. Its modular structure enables the user to define likelihoods for arbitrary processes and their corresponding final states – such as the example given in Equation (3) – and to also specify the detector model in the form of transfer functions for different objects. In addition, several minimization and integration algorithms can be used. The framework provides input and output interfaces to ASCII and ROOT files, and it can easily be adjusted to any analysis framework. The code is available on request.

KLFFitter has been developed for the case of top-quark reconstruction and its performance has been studied extensively [12–15]. It has been applied in a variety of physics analyses, see e.g. Refs. [1, 16–21]. The application to processes other than top-quark pair production is straight forward.

#### 4. Monte Carlo samples and detector modeling

The Monte Carlo sample used for the performance studies is generated using the Sherpa event generator [22–24] with the CTEQ6.6 [25] set of parton distribution functions and contains 5 million events. The simulated process is top-quark pair production with up to one additional parton in the final state, and subsequent decay via the single-electron decay mode. A center-of-mass energy of  $\sqrt{s} = 7 \text{ TeV}$  is assumed as well as a top-quark mass of  $m_{\text{top}} = 172.5 \text{ GeV}$ . Particle showering and hadronization are also performed using Sherpa. Particle jets are built with FastJet [26] using the anti- $k_t$  algorithm [27] with a radius parameter of  $R = 0.4$  and a minimum  $p_T$  of 15 GeV. Those particle jets are referred to as final-state particles throughout this paper. A matching criterion is added to associate jets at the particle level with partons using the distance between these objects defined as  $\Delta R = \sqrt{\Delta\eta^2 + \Delta\phi^2}$ , where  $\Delta\eta$  and  $\Delta\phi$  are the differences in pseudo-rapidity and azimuthal angle, respectively. This distance is required to be smaller than  $\Delta R = 0.3$ .

For simplicity, detector effects on the measured jets are modeled by sampling their energies from a Gaussian distribution centered around the particle-jet energies  $E$  [GeV] and with a standard deviation of  $\sigma/\text{GeV} = 0.65 \cdot \sqrt{E}/\sqrt{\text{GeV}} + 0.03 \cdot E/\text{GeV}$ . For the current example, the standard deviation is chosen to be independent of the type of the incident particle (light or heavy quark, gluon, or hadronically decaying tau lepton) and its pseudo-rapidity. The numerical values are chosen to roughly reflect the transfer functions used by the DØ collaboration [28]. The energies of charged leptons are smeared with  $\sigma/\text{GeV} = 0.1 \cdot \sqrt{E}/\sqrt{\text{GeV}}$ . The missing transverse momentum is defined as the negative sum of all matched jet and charged-lepton momenta.

Identification of  $b$  jets, *b-tagging*, is modeled by choosing a working point close to what can be found in the literature, see e.g. Refs. [1, 29]. The  $b$ -tagging efficiency – the probability to tag a jet containing a  $B$  hadron – is assumed to be 70%, the mis-tag rate – the probability to identify a non- $b$  jet as a  $b$  jet by mistake – is assumed to be 0.5%. Jets are  $b$ -tagged based on random numbers and on their true parton flavor. No assumptions are made on the underlying  $b$ -tag algorithm or on the output distributions of such an algorithm.

The transfer functions introduced in Section 2 are derived from the differences between the smeared jet energies and the energy of the particles at

the parton level. Figure 2 shows two examples, the distribution of  $(E_i^{\text{meas}} - E_i)/\sqrt{E_i}$  for  $b$  jets (left) and non- $b$  jets (right). The transfer functions for the  $\chi^2$ -method and the likelihood-based method are derived by fitting these distributions with single- and double-Gaussian functions, respectively. The fit range is constrained to the peak region for the  $\chi^2$ -method. Both parameterizations are indicated in the figure. Section 7 includes a discussion on how to implement more realistic transfer functions. We use the same parameterization for the transfer functions of charged leptons. On the contrary, transfer functions for the neutrinos are obtained from a single-Gaussian fit for both the  $\chi^2$ -method and the likelihood-based method.

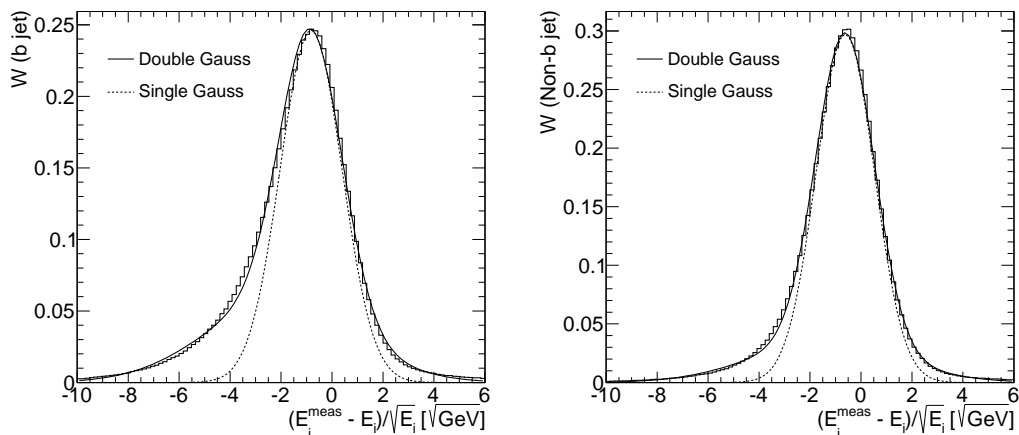


Figure 2: Transfer functions for  $b$  jets (left) and non- $b$  jets (right) shown as histograms, and the parameterization with a double-Gaussian and a single-Gaussian function. Note that, for this figure, the normalization of the single-Gaussian function is chosen such that it allows for a comparison of shapes.

## 5. Event selection

The selection of events is motivated by the signature of the single-lepton decay mode. The requirements for an event to be fitted are the presence of exactly one electron with  $p_T > 20$  GeV and  $|\eta| < 2.5$ , at least four jets with  $p_T > 20$  GeV and  $|\eta| < 2.5$ , and up to two  $b$ -tagged jets.

The fraction of events passing the selection, the *selection efficiency*, is about 19%. For each event, exactly four jets are considered in the kinematic

fit: first, all  $b$  jets are selected in order of their transverse momentum. Then the remaining (non- $b$ -tagged) jets are added, also sorted by their transverse momentum.

The set of jets considered in the kinematic fit does not always correspond to the final-state particles of the hard interaction. For example, this is due to initial- and final-state radiation, the chosen jet algorithm and acceptance cuts. In a *leading-order picture*, reconstructed jets can be associated with, or *matched* to, final-state particle jets by requiring their distance in  $(\eta - \phi)$ -space to be less than  $\Delta R = 0.3$ . The *matching efficiency* is defined as the fraction of events for which the four jets are unambiguously matched to the final-state particles. It is approximately 15% in the current example and further discussed in Section 6.1.

## 6. Performance studies

The performance of the three reconstruction algorithms is quantified based on two measures, the reconstruction efficiency and the reconstruction of top-quark properties. The *reconstruction efficiency* is defined as the fraction of matched events for which the chosen permutation is indeed the correct one. It is also defined separately for all objects or a subset of objects, e.g., the hadronically decaying  $W$  boson for which the two corresponding jets have to be identified correctly. These numbers are compared for the different reconstruction algorithms in Section 6.1 as a function of several kinematic quantities and also inclusively. The object reconstruction is quantified by the distribution of the difference between the reconstructed objects, e.g., the two top quarks, and the corresponding *truth* particles (calculated from the final-state particles). Three classes are compared in Section 6.2: matched events for which the chosen permutation is the correct one, all matched events and all selected events. The comparison of the first two classes shows the degradation from the ideal case of a completely efficient reconstruction algorithm to a less efficient algorithm, both applied to a set of events for which all selected jets can be associated with the final-state particles. The comparison of the second and third class shows the effect of including events for which such an association is not possible.

### 6.1. Reconstruction efficiencies

Table 1 shows the reconstruction efficiencies for the three algorithms under study, and those for the modified versions of the likelihood-based fit. The

first three rows give the probability to identify the correct permutation by chance ignoring any misidentification of  $b$  jets.

Table 1: The reconstruction efficiency for all jets (overall), the jets of the hadronically decaying  $W$  boson ( $W_{\text{had}}$ ) and the two  $b$  jets based on events produced at a center-of-mass energy of  $\sqrt{s} = 7$  TeV. The per-jet probability of correctly identifying a  $b$ -jet and the misidentification rate for light jets are also given. The first three rows indicate the reconstruction efficiencies determined from pure combinatorics ignoring misidentification. Numbers for the three different reconstruction algorithms without any extensions applied are presented in the next four rows. The further four rows represent these additional options which are subsequently included for the  $\chi^2$ - and the likelihood-based (LH) method. The last three rows show the the reconstruction efficiencies for the likelihood-based method including all extensions split into samples composed of events with zero, one and two  $b$ -tags. All efficiencies are calculated using matched events. The uncertainties are statistical uncertainties. Since the different methods are tested on the same data set, these uncertainties are correlated.

Method	Reconstruction efficiency [%]					
	Overall	$W_{\text{had}}$	$b_{\text{had}}$	$b_{\text{lep}}$	$p(b\text{-id})$	$p(b\text{-mis-id})$
Comb. 0-tag	8.3	16.7	25.0	25.0	50.0	50.0
Comb. 1-tag	16.7	33.3	33.3	33.3	66.7	33.3
Comb. 2-tag	50.0	100.0	50.0	50.0	100.0	0.0
$p_{\text{T}}^{\text{max}}$	$21.5 \pm 0.1$	$28.2 \pm 0.2$	$30.7 \pm 0.2$	$47.7 \pm 0.2$	$57.6 \pm 0.2$	$42.4 \pm 0.2$
$\chi^2$ ( $m_W$ con.)	$46.1 \pm 0.2$	$59.1 \pm 0.3$	$51.8 \pm 0.3$	$62.4 \pm 0.3$	$77.0 \pm 0.3$	$23.0 \pm 0.2$
$\chi^2$	$48.4 \pm 0.2$	$60.8 \pm 0.2$	$53.8 \pm 0.2$	$64.8 \pm 0.2$	$78.0 \pm 0.3$	$22.0 \pm 0.1$
Likelihood	$51.9 \pm 0.2$	$60.6 \pm 0.2$	$56.8 \pm 0.2$	$70.9 \pm 0.2$	$78.2 \pm 0.3$	$21.8 \pm 0.1$
$\chi^2 + b\text{-veto}$	$70.7 \pm 0.2$	$89.1 \pm 0.3$	$72.7 \pm 0.2$	$75.5 \pm 0.3$	$94.6 \pm 0.3$	$5.4 \pm 0.1$
LH+ $b\text{-veto}$	$74.3 \pm 0.3$	$88.8 \pm 0.3$	$76.4 \pm 0.3$	$79.5 \pm 0.3$	$94.4 \pm 0.3$	$5.6 \pm 0.1$
+fix mass	$83.3 \pm 0.3$	$91.1 \pm 0.3$	$84.9 \pm 0.3$	$88.0 \pm 0.3$	$95.5 \pm 0.3$	$4.5 \pm 0.1$
+angles	$83.8 \pm 0.3$	$91.2 \pm 0.3$	$85.3 \pm 0.3$	$88.4 \pm 0.3$	$95.6 \pm 0.3$	$4.4 \pm 0.1$
+0 $b$ -tag	$62 \pm 12$	$66 \pm 12$	$62 \pm 12$	$77 \pm 13$	$81 \pm 13$	$19 \pm 7$
+1 $b$ -tag	$75.9 \pm 0.4$	$81.7 \pm 0.4$	$79.1 \pm 0.4$	$85.8 \pm 0.4$	$90.8 \pm 0.4$	$9.2 \pm 0.1$
+2 $b$ -tag	$90.3 \pm 0.4$	$99.2 \pm 0.4$	$90.5 \pm 0.4$	$90.6 \pm 0.4$	$99.6 \pm 0.4$	$0.4 \pm 0.1$

All reconstruction efficiencies obtained with the  $p_{\text{T}}^{\text{max}}$ -method are smaller by factors of about 0.25-0.5 compared to those obtained with the  $\chi^2$ - and likelihood-based methods. This is expected as the latter two make use of more information of the top-quark decay topology and of the detector response. In particular, the  $p_{\text{T}}^{\text{max}}$ -method does not use information about the leptonically decaying top quark resulting in a large misidentification rate for

$b$  jets. The  $\chi^2$ -method with  $p'_z$  as an additional fit parameter instead of using a constraint on the  $W$ -boson mass ( $m_W$  con.) outperforms the other  $\chi^2$ -method by about 2% (absolute). The overall reconstruction efficiency obtained by the likelihood-based algorithm is about 4% larger than that obtained with the  $\chi^2$ -method. This difference can be explained by the modeling of the resonant decays (Breit-Wigner distributions compared to Gaussian distributions) and the more accurate parameterization of the transfer functions.

Using a veto for  $b$ -tagged jets which are interpreted as originating from light quarks results in an increase in the reconstruction efficiencies. In particular, the  $b$ -misidentification rate decreases significantly and, as a consequence, the probability to correctly identify the hadronically decaying  $W$  boson increases. This applies to both the  $\chi^2$ - and the likelihood-based method for which this  $b$ -veto is tested. The  $\chi^2$ -method in combination with a veto for  $b$ -tagged jets is similar to the reconstruction method used in Ref. [2], where only events with two  $b$ -tags are used. As expected, the overall reconstruction efficiency for the likelihood-based method is better by 4% and thus the remaining extensions are studied for this method only. Additionally fixing the top-quark mass to the value used in the simulated samples increases the reconstruction efficiencies even further due to the tighter constraints on the jet energies in comparison to the Breit-Wigner functions. The addition of angular information increases the efficiencies only slightly.

The presented numbers in the last three rows of Table 1 are based on a likelihood fit using all possible extensions and show that the reconstruction efficiency depends strongly on the number of  $b$ -tagged jets in an event. The reconstruction efficiencies rise from 62% for events without any  $b$ -tag (corresponding to a fraction of 0.03% of all matched events) to 75.9% (90.3%) for events with exactly one (two)  $b$ -tagged jets (corresponding to fractions of 46% and 54% of all matched events, respectively).

Figure 3 (left) shows the matching efficiencies, as defined as the fraction of events for which the four jets are unambiguously matched to the final-state particles, and (overall) reconstruction efficiencies for the likelihood-based algorithm (including the  $b$ -tag veto) as a function of the transverse momentum of the hadronically decaying top quark. The matching efficiency increases from about 10% at low  $p_T$  to roughly 25% at  $p_T \approx 500$  GeV, and it drops again for larger values. This drop can be explained by the fact that the decay products of the top quark are highly boosted and, in many cases, cannot be resolved by the jet algorithm. The reconstruction efficiency increases from about 50% at low  $p_T$  to about 90% at  $p_T \approx 250$  GeV and then remains con-

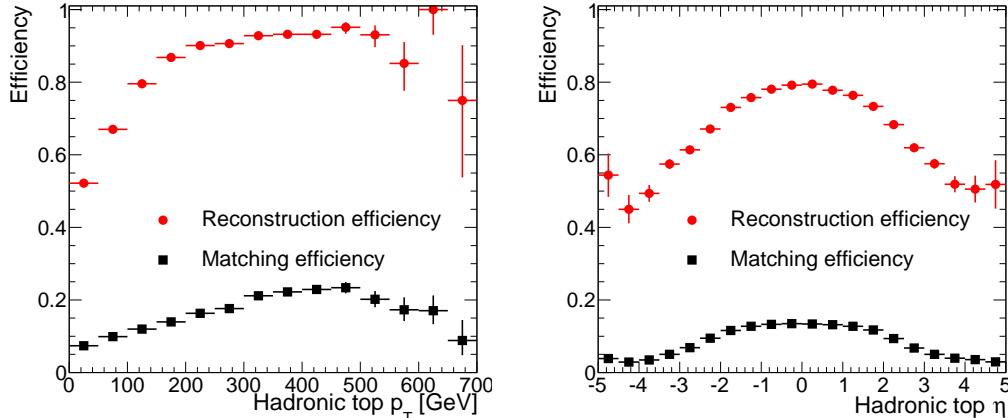


Figure 3: Matching and (overall) reconstruction efficiency for the likelihood-based reconstruction algorithm with the additional  $b$ -tag veto as a function of the transverse momentum (left) and the pseudo-rapidity (right) of the hadronically decaying top quark.

stant for higher  $p_T$  values. For large transverse momenta, it is less likely that a wrong combination of jets results in an invariant mass close to that of the top quark because the jets are strongly collimated compared to the case of low  $p_T$  values. Although high- $p_T$  top quarks can be reconstructed rather well, the fraction of events in which four resolved jets on the reconstruction level correspond to the particle-level jets is small.

Figure 3 (right) shows the two efficiencies as a function of the pseudo-rapidity of the hadronically decaying top quark. Both efficiencies are approximately constant in the central region, i.e.  $|\eta| < 1.5$ , and drop for larger values of  $|\eta|$ . This drop can be explained by the fact that the decay products of the top quark are more likely to be found outside the acceptance region of  $|\eta| < 2.5$ .

## 6.2. Object reconstruction

Figure 4 (left) shows the mass of the hadronically decaying top quark reconstructed with the three different algorithms using the full selected Monte Carlo data set. This mass is calculated using the invariant masses obtained from the jet energies. The distribution obtained by the  $p_T^{\max}$ -method is the broadest and peaks at around 160 GeV. The distributions obtained from the  $\chi^2$ - and the likelihood-based methods are significantly narrower and peak

closer to the top-quark mass assumed in the simulation. The tail to large masses is more pronounced for the  $\chi^2$ -reconstruction. For this comparison, the  $\chi^2$ -method treating the momentum components of the neutrino as free parameters is used.

The right-hand side of Figure 4 shows the same mass, but reconstructed with the likelihood-based algorithm (including the  $b$ -tag veto). Three different subsets of the Monte Carlo data set are considered: all events in the sample, matched events and matched events for which the correct permutation is chosen by the algorithm. The three distributions are normalized to unity. The latter distribution is approximately symmetric around the input mass while the distribution of all matched events has slightly larger tails due to the combinatorial background. The distribution for all events has a significant tail to larger mass values due to the combinatorial background and events in which not all final-state particles can be matched to the selected jets.

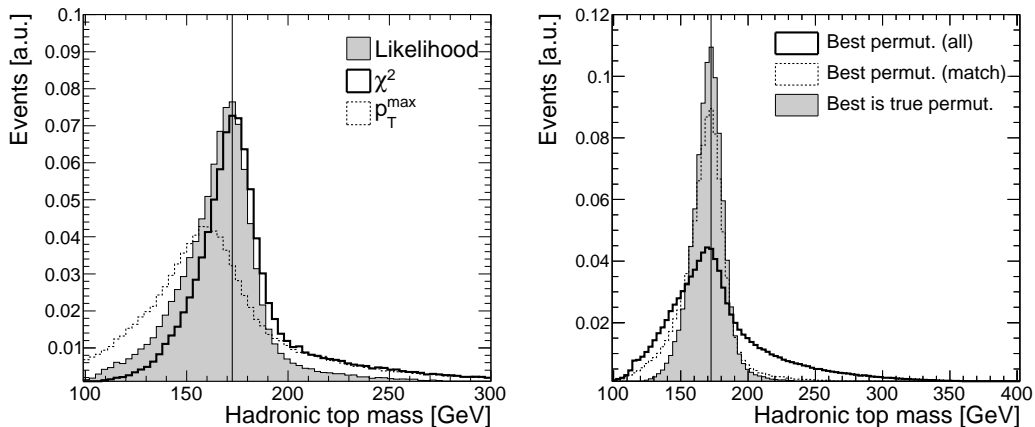


Figure 4: Mass of the hadronically decaying top quark reconstructed with the three different reconstruction algorithms using matched events (left) and with the likelihood-based algorithm including the  $b$ -tag veto (right) for three different subsets of the Monte Carlo data sample. The black line indicates the top-quark mass (physical parameter) assumed for the generation of Monte Carlo events.

Thus, two effects illustrate the impact of a more sophisticated reconstruction algorithm characterized by increased reconstruction efficiencies: the amount of combinatorial background is reduced since fewer top quarks are wrongly reconstructed and detector effects are reduced. Both effects lead

to a smaller and more distinct peak in the distribution of the reconstructed top-quark mass as shown in Figure 4.

Figure 5 (left) shows the  $\log \Delta R$  between the (true) hadronically decaying top quark and the reconstructed top quark for the three different reconstruction algorithms using only matched events. The distributions for all three algorithms show two peaks, one around  $\log \Delta R \approx -1$  and one around  $\log \Delta R \approx 0.5$ . The latter is due to combinatorial background while the former reflects the resolution with which particle-level top quarks can be matched to reconstructed top quarks. As expected, the peak at smaller values is more pronounced for the likelihood-based approach. Figure 5 (right) shows  $\log \Delta R$  for events reconstructed with the likelihood-based algorithm including the  $b$ -tag veto for three different subsets of the Monte Carlo data sample. Matched events for which the chosen permutation corresponds to the true one have a peak around  $\log \Delta R \approx -1$ . The distribution of all events raises continuously and peaks at  $\log \Delta R \approx 0.5$  due to the quasi-random assignment of jets to the hadronically decaying top quark.

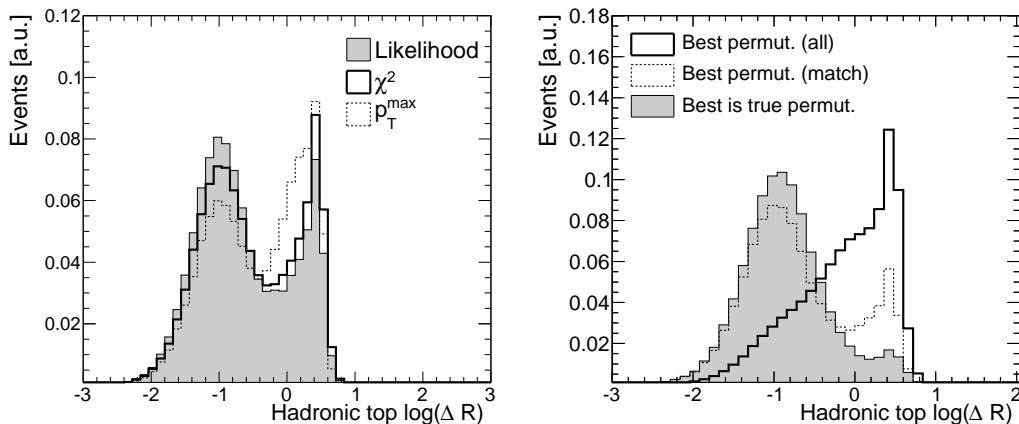


Figure 5: The distance  $\log \Delta R$  between the (true) hadronically decaying top quark and the one reconstructed with the three different reconstruction algorithms using matched events (left) and with the likelihood-based algorithm including the  $b$ -tag veto (right) for three different subsets of the Monte Carlo data sample.

## 7. Discussion

### 7.1. Summary

We presented a flexible framework for kinematic fitting which can be applied to arbitrary event topologies and models. For the performed studies, a likelihood-based reconstruction algorithm was introduced and its performance was compared to that of two commonly used algorithms for the case of top-quark pair production. It was found that the likelihood-based algorithm results in the largest reconstruction efficiency because of a more accurate description of the underlying physics process and detector effects.

Although this algorithm performs best at moderate to large transverse top-quark momenta, the matching efficiency drops in that regime indicating that a different class of algorithms has to be used to reconstruct boosted top-quark pairs, see e.g. Refs. [30–34].

If more than four jets are considered in the fit, the number of ways to associate four jets out of the selected ones with the final-state particles increases. This increases the matching efficiency because the probability to select those jets corresponding to the final-state particles increases. On the other hand, the reconstruction efficiency decreases because it becomes more likely to fulfill the constraints in Equation 3 by chance for permutations with a wrong assignment of jets, see Ref. [15].

Different types of likelihood-based reconstruction algorithms in KLFitter have been successfully applied in a variety of physics analyses.

### 7.2. Future developments

The transfer functions used by the  $\chi^2$  and likelihood-based algorithms are assumed to not depend on the particle's properties, and only a rough distinction is made between light and  $b$  jets. In a real experiment, however, the energy measured in the calorimeter indeed depends on those specifications. For example, jets originating from light quarks or gluons will differ in their shape and visible energy compared to jets containing  $B$  hadrons. The latter also might need to be categorized according to the decay of the  $B$  hadron because leptonic decays of  $B$  mesons result in neutrinos which carry away some of the energy of the jet. Furthermore, the quality of the jet reconstruction may depend on the pseudo-rapidity as different detector components may be used for the reconstruction. More realistic transfer functions can also be obtained by considering the energy dependence of the parameterization of

these functions. Apart from that, further studies may investigate the impact of pile-up effects on the matching and the reconstruction efficiencies.

Future developments also include a refinement of the likelihood using, e.g., the leading-order matrix element for top-quark pair production and decay or the pole mass distributions from the  $W$  boson and the top quark as obtained from truth Monte Carlo.

### *7.3. Outlook*

As an outlook to the running of the LHC with an increased center-of-mass energy and in view of the increased pile-up, the studies are repeated with Monte Carlo simulations assuming a center-of-mass energy of  $\sqrt{s} = 14$  TeV. The same transfer functions are used as for the 7 TeV study.

The selection efficiency of this sample amounts to about 16%. As the average transverse momentum of the top quarks increases, the matching efficiency decreases to roughly 13%. On the other hand, and consistent with Figure 3 (left), the different reconstruction efficiencies for matched events increase by about 2 – 3%. The corresponding numbers for the tested reconstruction algorithms are listed in Table 2. Likelihood-based fitting will hence also be valuable for future measurements at the LHC.

## **Acknowledgements**

We would like to thank all users of KLFitter who helped to improve the package. We are also very thankful to Steffen Schumann for his support in the event generation with Sherpa.

Table 2: The reconstruction efficiency for all jets (overall), the jets of the hadronically decaying  $W$  boson ( $W_{\text{had}}$ ) and the two  $b$  jets based on events produced at a center-of-mass energy of  $\sqrt{s} = 14$  TeV. The per-jet probability of correctly identifying a  $b$ -jet and the misidentification rate for light jets are also given. The first three rows indicate the reconstruction efficiencies determined from pure combinatorics ignoring misidentification. Numbers for the three different reconstruction algorithms without any extensions applied are presented in the next four rows. The further four rows represent these additional options which are subsequently included for the  $\chi^2$ - and the likelihood-based (LH) method. The last three rows show the the reconstruction efficiencies for the likelihood-based method including all extensions split into samples composed of events with zero, one and two  $b$ -tags. All efficiencies are calculated using matched events. The uncertainties are statistical uncertainties. Since the different methods are tested on the same data set, these uncertainties are correlated.

Method	Reconstruction efficiency [%]					
	Overall	$W_{\text{had}}$	$b_{\text{had}}$	$b_{\text{lep}}$	$p(b\text{-id})$	$p(b\text{-mis-id})$
Comb. 0-tag	8.3	16.7	25.0	25.0	50.0	50.0
Comb. 1-tag	16.7	33.3	33.3	33.3	66.7	33.3
Comb. 2-tag	50.0	100.0	50.0	50.0	100.0	0.0
$p_{\text{T}}^{\text{max}}$	$23.6 \pm 0.2$	$29.8 \pm 0.2$	$31.9 \pm 0.2$	$52.4 \pm 0.2$	$59.2 \pm 0.2$	$40.8 \pm 0.2$
$\chi^2$ ( $m_W$ con.)	$48.1 \pm 0.3$	$61.5 \pm 0.3$	$53.2 \pm 0.3$	$64.3 \pm 0.3$	$78.5 \pm 0.3$	$21.5 \pm 0.2$
$\chi^2$	$50.0 \pm 0.3$	$62.7 \pm 0.3$	$54.8 \pm 0.3$	$66.4 \pm 0.3$	$79.2 \pm 0.3$	$20.8 \pm 0.2$
Likelihood	$55.0 \pm 0.3$	$62.7 \pm 0.3$	$59.3 \pm 0.3$	$74.5 \pm 0.3$	$79.5 \pm 0.3$	$20.5 \pm 0.2$
$\chi^2$ + $b$ -veto	$71.6 \pm 0.3$	$89.9 \pm 0.3$	$73.4 \pm 0.3$	$76.1 \pm 0.3$	$94.9 \pm 0.3$	$5.1 \pm 0.1$
LH+ $b$ -veto	$77.1 \pm 0.3$	$89.7 \pm 0.3$	$78.9 \pm 0.3$	$82.2 \pm 0.3$	$94.8 \pm 0.3$	$5.2 \pm 0.1$
+fix mass	$85.1 \pm 0.3$	$92.0 \pm 0.3$	$86.5 \pm 0.3$	$89.6 \pm 0.3$	$96.0 \pm 0.3$	$4.0 \pm 0.1$
+angles	$85.6 \pm 0.3$	$92.1 \pm 0.3$	$86.9 \pm 0.3$	$90.0 \pm 0.3$	$96.1 \pm 0.3$	$3.9 \pm 0.1$
+0 $b$ -tag	$72 \pm 15$	$75 \pm 16$	$75 \pm 16$	$88 \pm 17$	$84 \pm 16$	$16 \pm 7$
+1 $b$ -tag	$78.6 \pm 0.4$	$83.7 \pm 0.4$	$81.2 \pm 0.4$	$87.9 \pm 0.5$	$91.8 \pm 0.4$	$8.2 \pm 0.1$
+2 $b$ -tag	$91.4 \pm 0.4$	$99.2 \pm 0.4$	$91.6 \pm 0.4$	$91.8 \pm 0.4$	$99.6 \pm 0.4$	$0.4 \pm 0.1$

## References

- [1] ATLAS Collaboration, Eur. Phys. J. C 72 (2012) 2046.
- [2] CMS Collaboration, JHEP 12 (2012) 105.
- [3] DØ Collaboration, Phys. Rev. D 83 (2011) 032009.
- [4] CDF Collaboration, Phys. Rev. D 87 (2013) 092002.

- [5] D. Binosi, J. Collins, C. Kaufhold, L. Theussl, *Comput. Phys. Commun.* 180 (2009) 1709.
- [6] ATLAS Collaboration (2009). arXiv:0901.0512.
- [7] P. Weigell (2009). Diploma thesis, Munich, MPP-2009-177.
- [8] S. S. Snyder (1995). PhD thesis, FERMILAB-THESIS-1995-27.
- [9] L. Lyons, *Statistics for Nuclear and Particle Physicists*, Cambridge University Press, 1989.
- [10] A. Czarnecki, J. G. Korner, J. H. Piclum, *Phys. Rev. D* 81 (2010) 111503.
- [11] A. Caldwell, D. Kollar, K. Kröninger, *Comput. Phys. Commun.* 180 (2009) 2197.
- [12] E. Fuchs (2009). Bachelor thesis, II.Physik-UniGö-Bach-2009/07.
- [13] S. Ebert (2010). Bachelor thesis, II.Physik-UniGö-Bach-2010/01.
- [14] P. Stolte (2010). Bachelor thesis, II.Physik-UniGö-Bach-2010/02.
- [15] O. Nackenhorst (2010). Diploma thesis, II.Physik-UniGö-Dipl-2010/04.
- [16] ATLAS Collaboration, *Eur. Phys. J. C* 72 (2012) 2039.
- [17] ATLAS Collaboration, *JHEP* 1206 (2012) 088.
- [18] ATLAS Collaboration, *Phys. Rev. Lett.* 108 (2012) 261802.
- [19] ATLAS Collaboration, *Phys. Rev. D* 86 (2012) 091103.
- [20] ATLAS Collaboration, *Eur. Phys. J. C* 73 (2013) 2261.
- [21] ATLAS Collaboration, *Phys. Rev. Lett.* 111 (2013) 232002.
- [22] T. Gleisberg, et al., *JHEP* 0902 (2009) 007.
- [23] S. Hoeche, F. Krauss, S. Schumann, F. Siegert, *JHEP* 0905 (2009) 053.
- [24] S. Schumann, F. Krauss, *JHEP* 0803 (2008) 038.
- [25] P. M. Nadolsky, et al., *Phys. Rev. D* 78 (2008) 013004.

- [26] M. Cacciari, G. P. Salam, G. Soyez, *Eur. Phys. J. C* 72 (2012) 1896.
- [27] M. Cacciari, G. P. Salam, G. Soyez, *JHEP* 0804 (2008) 063.
- [28] V. M. Abazov, et al., *Phys. Rev. D* 84 (2011) 032004.
- [29] CMS Collaboration, *JINST* 8 (2013) P04013.
- [30] D. E. Kaplan, K. Rehermann, M. D. Schwartz, B. Tweedie, *Phys. Rev. Lett.* 101 (2008) 142001.
- [31] J. Thaler, L.-T. Wang, *JHEP* 0807 (2008) 092.
- [32] T. Plehn, M. Spannowsky, M. Takeuchi, D. Zerwas, *JHEP* 1010 (2010) 078.
- [33] ATLAS Collaboration, *JHEP* 1301 (2013) 116.
- [34] CMS Collaboration, *JHEP* 1209 (2012) 029.